Available online at www.CivileJournal.org

Civil Engineering Journal

(E-ISSN: 2476-3055; ISSN: 2676-6957)

Vol. 10, No. 05, May, 2024

GGBFS and Red-Mud based Alkali-Activated Concrete Beams: Flexural, Shear and Pull-Out Test Behavior

Hebah M. Al-Jabali [1], Ahmed A. El-Latief [2], Mohamed Salah Ezz [3*], Shady Khairy [2], Amr. A. Nada [2]

[1] *Department of Civil Engineering, Hijjawi Faculty for Engineering Technology, Yarmouk University. P.O. Box 566, Irbid 21163, Jordan.*

[2] *Department of Civil Engineering, Higher Technological Institute, 10th of Ramadan City, Egypt.*

[3] *Department of Architecture, The Higher Institute for Engineering and Technology, Obour City - K21 Cairo/Bilbies Rd, Egypt.*

Received 15 February 2024; Revised 12 April 2024; Accepted 19 April 2024; Published 01 May 2024

Abstract

Geopolymers and antacid-enacted fasteners have accumulated critical interest as promising development and fixing materials because of their exceptional properties. Also, they bring about less contamination contrasted with regular concrete cements. Geopolymers address a clever class of suggested restricting materials blended through the basic enactment of bountiful aluminosilicate materials. The usage of geopolymer materials from side effects offers a critical decrease in carbon impression and yields positive natural effects. Geopolymer is progressively recognized as a plausible substitute for OPC concrete. In this review, sodium-based antacid activators, especially sodium metasilicate (Na_2SiO_3), were used for different blend extents. The boundaries researched included NaOH arrangements with a grouping of 8 M, alongside a Na_2SiO_3/NaOH proportion of 1. This paper evaluates the fundamental characteristics of geopolymer cement beams, employing red mud and GGBFS in powdered form as complete replacements for traditional concrete. Six bar specimens are tested under a two-point static loading condition, all cured at room temperature under ambient conditions. Of the six beams, three were exposed to flexural conduct testing with a molarity of 8 M, while the excess three beams were tried for shear conduct. The outcomes of testing geopolymer beams subjected to shear and bending loads indicated that the beams incorporating aluminum slag performed better than those incorporating blast furnace slag. Both types also demonstrated promising results compared to beams incorporating OPC, highlighting their potential environmental benefits compared to cement use.

Keywords: Geopolymer Beams; Alkali Activator; Flexural; Shear; Pull-Out; GGBFS; Red-Mud.

1. Introduction

Due to the rapid progress in global infrastructure development, there has been a significant increase in the demand for construction materials. However, in today's era of sustainable development, it is crucial to adhere to standards that extend beyond the long-term performance of these materials [1]. Notwithstanding the significant worldwide use of cement yearly, determined concerns remain in regard to the manageability of substantial parts and the strength of substantial designs presented to serious ecological circumstances [2]. Moreover, economic and environmental considerations are gaining increasing significance. Portland cement, a commonly used construction material, is known for its high energy consumption. The focus on reducing greenhouse gas emissions through global initiatives and conferences has stimulated the adoption of supplementary cementitious materials (SCMs) as alternatives to traditional

* Corresponding author: drmohamedsalah@oc.edu.sa

http://dx.doi.org/10.28991/CEJ-2024-010-05-09

cement binders [1, 3, 4]. The progression of geopolymer innovation comes from significant examination tries pointed toward making elective covers from minimal expense with modern side-effects. These covers show properties practically identical to or even better than those of customary concrete folios [1, 5, 6]. It's generally recognized that the most restricting part of conventional Portland concrete is calcium silicate hydrate (CSH) [7]. Then again, geopolymers show a three-layered aluminosilicate network as the essential construction of the fastener [1, 4]. The creation of geopolymer covers includes the polymerization response of aluminosilicate species, commonly depicted by the recipe Mn-[[-Si-O_2] z-AlO] n. wH_2O [8, 9]. Here, M represents the alkaline component, while z indicates the degree of polymerization. Various studies have demonstrated enhanced properties of geopolymers when alkaline activators based on sodium (Na) or potassium (K) are employed [1, 10, 11].

Monomers collaborate to shape oligomers, which then, at that point, advance to make a three-layered organization of aluminosilicate structures, as framed by Davidovits in 1994 [12]. The process of dissolution and polycondensation is referred to as geo-polymerization (Figure 1). Positive ions play a vital role within the system to neutralize the negative charge of aluminum ions in IV-fold coordination, as emphasized by previous studies [10, 13, 14]. As research advances, there has been a concerted effort to explore the characteristics of geopolymer mortar and concrete produced using alkaline activators and various aluminosilicate source materials such as kaolin (KL), metakaolin (MK), fly ash (FA), slag, and other industrial by-products. In recent times, to enhance the utilization of geopolymers in the construction sector, numerous researchers have dedicated significant efforts to improving the mechanical strength and durability of geopolymer concrete. This frequently entails the incorporation of aluminosilicate additives or even organic additives.

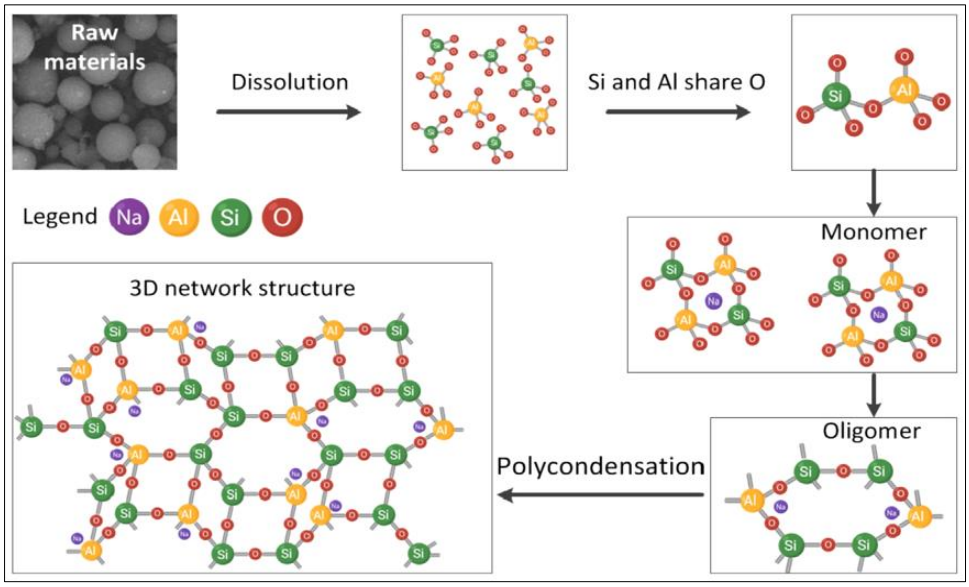

Figure 1. Geopolymerization process [12]

Alkali-activated binders are produced through various chemical reactions initiated by a base attacking amorphous, or semi-crystalline, or crystalline aluminosilicate precursors derived from industrial by-products or natural materials. Commonly used alkaline activators include MOH and $M_2O.rSiO_2$, where M represents either Na or K [2, 10]. Different activators, like M_2CO_3, M_2SO_3, M_3PO_4, MF, $M_2O.nAl_2O_3$, M2O.Al_2O3. (2-6) SiO_2, and M_2SO_4, have been utilized to various degrees. The aluminosilicate forerunners can be grouped by their calcium oxide content into two classes: high-calcium and low-calcium antecedents [2, 10, 15]. The advancement of Alkali-Activated Binders (AABs) commenced with the activation of high-calcium precursors, notably ground-granulated blast furnace slag. This approach was later expanded to incorporate low-calcium precursors, with industrial pozzolans such as fly ash being extensively utilized, although the utilization of metakaolin, natural pozzolans, and agricultural waste by-products remains somewhat limited. It is generally recognized that every class of AABs offers unmistakable benefits, especially concerning solidity [2, 16, 17].

Previous studies introduced a theoretical framework proposing significant interactions between salts and cementitious materials. This hypothesis gained traction and laid the groundwork for the development of a new class of materials, initially referred to as "alkaline-activated concretes" [18, 19]. In high-calcium Alkali-Activated Binders (AABs), the primary reaction product is C-A-S-H or C-(N)- A-S-H, which significantly enhances the chemical binding of water, consequently reducing permeability. When discussing salt-activated binders, C, N, A, S, and H correspond to CaO, Na_2O, Al_2O_3, SiO_2, and H_2O, respectively, employing the notation commonly utilized in concrete science documentation. [1, 2, 10, 20]. Moreover, the alkali-silica reaction (ASR) is a well-recognized concern in cement and mortars based on ordinary Portland cement (OPC). This phenomenon arises from the interaction between reactive

siliceous phases found in the fine/coarse aggregates and the hydroxyl ions in the pore structure of the cement paste. For ASR to show and persevere, three basic circumstances should be satisfied: adequate dampness (something like 80% relative mugginess inside the substantial), raised alkalinity, and the presence of responsive siliceous stages in the totals [15, 21]. The ASTM standard test techniques for evaluating salt silica reactivity in totals and concrete, for example, ASTM C 227, C 1293, C 1260, and C 1567, use extension as the fundamental mark of ASR [4, 22]. According to Davidovits [12], alkali-activated class C fly ash mortars displayed shrinkage under ASTM C 227, though OPC mortars, tried under indistinguishable circumstances, showed huge development. In 1988, Davidovits [12] identified an alkaline activator solution capable of reacting with silicon and aluminum in materials of terrestrial origin, as well as with by-products such as fly ash and rice husk ash, to produce binders [6, 12]. The term 'geopolymer' was acquainted to mean these limiting materials. Geopolymer concrete (GPC) is a kind of substantial that takes out the dependence on regular concrete in its assembling cycle. [13, 18]. Geopolymer concrete (GPC) has drawn extensive interest from specialists attributable to its promising potential when contrasted with common Portland concrete (OPC) [23–25]. There is presently a change in research center from science to design, with an emphasis on investigating the business creation of GPC [2, 12, 15].

A few modern side-effects can act as options in contrast to customary concrete, including fly debris, ground-granulated impact heater slag, lead smelter slag, and glass sand, among others. These materials show equivalent or predominant strength and toughness properties, in this manner supporting decreasing the carbon impression and tending to the difficulties related to modern garbage removal [15, 26]. The alkaline activating solution, composed of sodium or potassium silicates and hydroxides, interacts with the alumina-silica present in the source material. In a perfect world, this response happens under raised restoring temperatures going from 50 to 100 °C, bringing about the development of polymerization items. Furthermore, numerous specialists prefer to utilize the term antacid-initiated material (AAM) rather than geopolymer while examining materials with modern side effects attributable to the salt enactment of alumina-silicate source materials [27–29].

A significant difference observed in the chemistry of geopolymers compared to conventional concrete binders is the absence of calcium content in the resulting polymerization product. This is attributed to the non-participation of calcium silicate hydrate (CSH) in the polymerization process [16, 30]. Geopolymer concrete is created using different modern results and is dependent upon assorted relieving conditions. The expansion of GGBS to fly debris has altogether improved the compressive strength of geopolymer concrete [6, 16, 31]. The grouping of the activator impacts both the strength properties and the setting season of the substance. The incorporation of nano-SiO_2 and nano-Al_2O_3 into fly ash has demonstrated improvements in the performance of geopolymer concrete. Self-healing properties in geopolymer can be attained by incorporating Terminalia chebula and palm jaggery into blends of fly ash and ground granulated blast furnace slag [6, 16, 30]. Broiler-relieving of geopolymer concrete at various temperatures affects its compressive strength. The decision on response items impacts the mechanical properties of geopolymer concrete [6]. High calcium fly debris geopolymer mortar displays further development in terms of stream, strength, and drying shrinkage [6, 31]. Incorporating mineral admixtures, such as silica fume, enhances the flexural strength of concrete. Additionally, incorporating a binder containing up to 5% slaked lime in geopolymer concrete, alongside fly ash and GGBS, improves the mechanical properties of the concrete [6, 18, 31, 32].

The term 'geopolymer' was familiar with portraying these fasteners [13]. Geopolymer concrete (GPC) is a type of concrete that eliminates the need for conventional Portland cement in its production. GPC has garnered significant attention from researchers due to its promising potential compared to traditional Portland cement (OPC) [10, 13]. The mechanical strength of the GPC framework is affected by different elements [18]. The fundamental component impacting the compressive strength of GPC is the pH level of the initiating arrangement, as verified by Hemn Qader Ahmed Khale et al. [18, 26]. An activating solution within the pH range of 13–14 is considered optimal for achieving GPC with enhanced mechanical strength. Moreover, the properties of the source materials also influence the strength of GPC; materials with high reactivity yield geopolymer systems with higher compressive strength. Then again, improving the early strength advancement of the geopolymer framework can be accomplished by using NaOH with higher molarity, even with decreased antacid substance, and by forcing the restoring system to raise temperatures [5, 7, 13, 33].

In the wake of directing trials and scientific examinations on RFT geopolymer Portland concrete cement (RGPC) radiates and ordinary Portland concrete cement (RPCC) radiates, it tends to be deduced that the heap diversion attributes of both RGPC and RPCC radiates are practically vague [34–36]. The flexural capacity and service load capacity exhibited a slight decrease in RGPC beams compared to RPCC beams. Additionally, the study indicated that while the ultimate moment capacity of RGPC beams exceeded that of RPCC beams due to their higher compressive strength, the standardized moment capacity analysis revealed lower breaking and service load moments for RGPC beams, albeit with a similar ultimate moment capacity [10, 34]. The comparison of the flexural behavior between Geo-Polymer Concrete (GPC) beams and conventional cement beams led to the following conclusions: Geopolymer concrete demonstrates enhanced mechanical properties compared to conventional cement of similar grade. The GPC beams show higher initial failure load and ultimate load values compared to conventional cement beams, indicating a superior load-bearing capacity for the former. Additionally, both types of beams fail in flexural mode, with the failure of GPC beams exhibiting

greater ductility compared to that of conventional cement beams, characterized by significant crushing in the compression zone. GPC beams exhibit a higher occurrence of fine cracks with tighter spacing compared to conventional cement beams, meeting workability standards.

Moreover, the energy absorption capacity of GPC beams is generally higher than that of conventional cement beams, attributed to their enhanced load-bearing capacity and larger deflections, indicating improved ductility. Additionally, the flexural toughness index of GPC beams is slightly better compared to that of traditional cement beams, and the experimental study suggests that geopolymer concrete exhibits enhanced properties compared to conventional cement, with its behavior aligning with that of ordinary cement [20, 22, 37]. Through exploratory examinations [10, 35], it was demonstrated that determining the optimal replacement level of fly ash with Ground Granulated Blast Furnace Slag (GGBS) in Geo-Polymer Concrete (GPC) is not definitive. The water absorption property is lower than that of conventional cement. Furthermore, the objective of rapidly achieving strength, particularly reaching 70% of the compressive strength within the initial 4 hours of setting, was successfully attained. The study aimed to evaluate the various strength properties of geopolymer concrete with varying percentages of GGBS substitution. Several investigations have explored the flexural strength of steel-reinforced GPC (SRGPC) beams. The load-deflection relationship observed in steel-reinforced OPC (SROPC) and SRGPC beams exhibits remarkable similarity, albeit with a slightly greater ultimate load in SRGPC beams [38]. The underlying breaking heap of SRGPC radiates outperforms that of SROPC radiates, showing an unrivaled burden-bearing limit. Moreover, the disappointment of SRGPC radiates illustrates improved malleability contrasted with SROPC radiates, as described by a more noteworthy event of fine breaks. The concentrate on glass fiber-built-up polymer-RGPC radiates found that the width of the bars didn't prominently impact the flexural strength of the pillars [18, 37, 39]. In addition, expanding the rebar proportion further developed the workableness conduct of the bars.

In this continuing study, static load tests were conducted to analyze the flexural and shear performance of six geopolymer reinforced concrete (GRC) beams. Three concrete beams were subjected to testing for their ability to withstand tensile stresses, utilizing the optimal concentration for geopolymer concrete, specifically 8 moles. In a parallel set of experiments, three beams underwent testing to evaluate the performance of geopolymer concrete in resisting bending stresses, maintaining the same concentration of alkalis. Furthermore, the identical concrete samples were assessed for their slip resistance. The research examined the viability of reinforcing shear and flexural strength using RFT, based on experimental findings, and measured the influence of variables such as the quantity and diameter of steel bars and binder. Ultimately, a refined predictive model was suggested to assess the shear, flexural, and slip capacities of GRC beams. Also, Figure 2 briefly shows the process of the methodology.

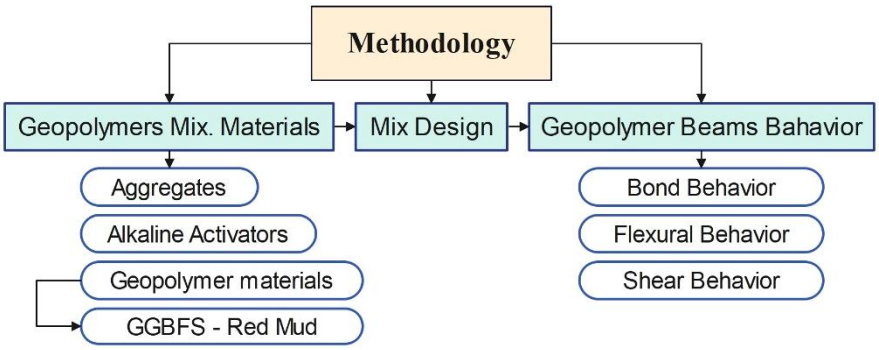

Figure 2. Research methodology flowchart

1.1. Research Significance

This study provides experimental findings aimed at assessing the shear and bending strengths of geopolymer concrete beams composed of ground-granulated blast furnace slag GGBFS and aluminum slag RM (red mud) following conventional treatment methods. Additionally, the research investigates the resistance of polymer concrete, derived from blast furnace slag and aluminum slag, to sliding stress:

The examination of geopolymer concrete, considered a promising form of eco-friendly concrete, is structured around several key aspects, which include:

Sustainable Construction Materials: Experimentation with geopolymer concrete, particularly utilizing blast furnace slag and aluminum slag, contributes to the development of sustainable construction materials. These industrial by-products can be repurposed, reducing the environmental impact of waste disposal.

Reduced Carbon Footprint: Concrete in geopolymer conditions presents a substitute for conventional concrete based on Portland cement, which is a significant source of carbon emissions. By using blast furnace slag and aluminum slag, experiments aim to reduce the carbon footprint associated with concrete production.

***Enhanced Performance Characteristics**:* Alkaline solutions serve as activators in geopolymer concrete, facilitating rapid strength development and improved durability. By conducting experiments, scientists can evaluate the mechanical attributes and resilience of geopolymer concrete, ultimately enhancing its efficacy in diverse structural uses.

***Cost-effectiveness**:* Utilizing industrial by-products such as blast furnace slag and aluminum slag in geopolymer concrete can potentially lower production costs compared to traditional concrete. Experimental studies help evaluate the cost-effectiveness of geopolymer concrete, making it an economically viable option for construction projects.

***Innovation and Advancement**:* Experimentation fosters innovation and advancement in construction materials. By exploring the properties and behavior of geopolymer concrete, researchers can identify opportunities for improvement and develop new formulations tailored to specific engineering requirements.

***Environmental Benefits**:* Geopolymer concrete production emits fewer greenhouse gases and consumes less energy compared to Portland cement-based concrete. Conducting experiments on geopolymer concrete contributes to reducing environmental pollution and conserving natural resources.

***Promoting Circular Economy**:* Incorporating industrial by-products into geopolymer concrete supports the principles of a circular economy by minimizing waste generation and promoting resource efficiency. Experiments demonstrate the feasibility and benefits of incorporating these materials into construction practices.

2. Material and Methods

This part frames the trial program for this review, including a prologue to the materials used and their consistency with ASTM determinations. The examination investigates the usage of completely supplanting concrete materials or geo-polymer materials, for example, GGBFS and red mud (aluminum slag), which were inspected and utilized as geo-polymer fasteners. The objective is to develop a novel, environmentally friendly concrete with sufficient strength, thereby promoting the eco-friendliness and sustainability of the concrete industry.

2.1. Aggregate

The substantial used normal total (NA), containing coarse total (CA), including squashed dolomite with a NMS of 19 mm, and regular sand (FA) with a particular gravity of 2.58. The fine total, going in size from 0.15 to 1.2 mm, was utilized for all substantial blends in the underlying set. The pre-owned normal sand agrees with standard determination ASTM C33/C33M [40]. The size circulation of the normal coarse total (CA) and fine total (FA) used is portrayed in Figure 3, while their separate physical and mechanical properties are itemized in Table 1.

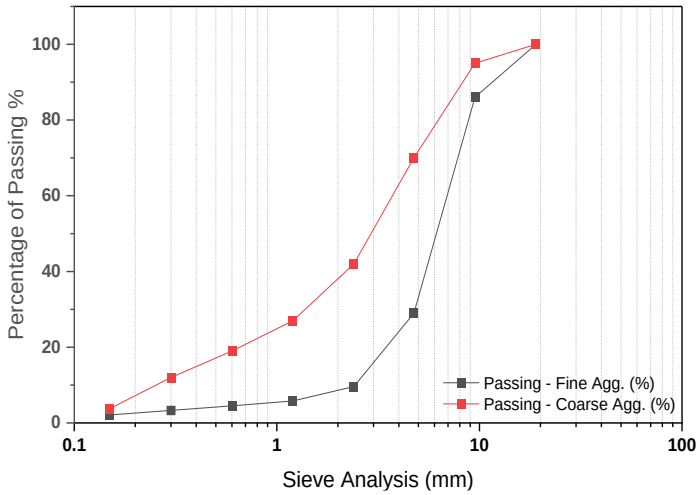

Figure 3. Particle size distribution for (CA) and (FA)

Table 1. Coarse aggregate (CA) and fine aggregates (FA) Properties

values	NA – Nat. Agg.	
	Coarse aggregates (CA)	Fine aggregates (FA)
Los Angeles abrasion %	17.56	-
Crushing value %	17.93	-
Water absorption %	0.86	1.9
Specific gravity	2.65	2.58
Volume density	1430	1612

2.2. Portland Cement (PC)

The review utilized Portland concrete (CEM 42.5 N), described by a particular gravity of 3.14 g/cm^3 and a particular surface area of 3000 cm^2/gm. Also, the fly debris (FA) utilized was gathered from the Sika organization for the development synthetics in Egypt. As per ASTM C618-12a principles [41], fly debris is arranged into two unmistakable classes: low-calcium FA (Class F) and high-calcium FA (Class C). Low-calcium FA was used. The structure of OPC and FA is expounded in Table 2, while Table 3 portrays their actual qualities.

Table 2. OPC, Red-Mud, and GGBFS Chemical composition

Material	SiO_2	CaO	Al_2O_3	Fe_2O_3	MgO	K_2O	Na_2O
OPC	20.9	62	6.2	3.2	3.3	-	-
Red-Mud	23.6	6.18	56.8	2.99	2.27	0.61	0.65
GGBFS	34	43.3	9.3	3.01	4.49	0.5	0.73

Table 3. Physical composition of component materials

Materials	Properties
GGBFS	Specific gravity: 2.15 g/cm^3 Specific surface area: 6150 cm^2/g Soundness: 1 mm Color: off-white
Red-Mud	Specific gravity: 2.65 g/cm^3 Specific surface area: 5200 cm^2/g Soundness: 1.12 mm Color: dark-grey
Cement	Specific gravity: 3.14 g/cm^3 Specific surface area: 3000 cm^2/g

2.3. Geopolymer Materials

Materials derived from manufacturing processes, such as industrial by-products from the aluminum and iron industries, offer potential as alternatives to cement in concrete structures. These materials, including aluminum slag and ground granulated blast furnace slag (GGBFS), possess properties conducive to cement replacement. Studies highlight their pozzolanic activity when activated with alkaline solutions, indicating their viability in geopolymer concrete. This sustainable approach not only utilizes abundant industrial waste but also reduces environmental impact by decreasing cement consumption. By exploring these alternative materials, the construction industry aims to enhance sustainability and resource efficiency while maintaining structural integrity and performance. GGBFS and Red-Mud were selected from manufacturing processes, and their potential as complete substitutes for cement was assessed by examining the properties of each.

2.3.1. Ground Granulated Blast Furnace Slag, GGBFS

Ground Granulated Blast Furnace Slag (GGBFS) was obtained from Suez Steel Organization in Suez, Egypt. Its qualities incorporate a particular gravity of 2.48 g/cm³, volumetric load of 2.15 g/cm³, explicit surface area of 6150 cm²/g, and sufficiency of 1.00 mm. Figure 3 portrays the molecule-size circulation of GGBFS, which displays a dull, dim hue. Table 2 presents the substance creation of Red Mud, while Table 3 frameworks its actual properties.

2.3.2. Aluminum Slag (Red-Mud)

Red-Mud, obtained from various aluminum organizations like Mit-Ghamr, Dakahlia, Egypt (for example, Alenairy Organization for Aluminum Organization, Ismail Metal Working Organization, among others), is described by a particular gravity of 2.65 g/cm^3, volumetric load of 1.18 g/cm^3, explicit surface area of 5200 cm^2/gm, and sufficiency of 1.12 mm. The molecule-size conveyance of Red-Mud is portrayed in Figure 3, displaying its dim hue. Table 2 gives a point-by-point outline of the compound synthesis of Red-Mud, while its actual properties are portrayed in Table 3. Both GGBFS and Red-Mud (aluminum slag) are portrayed as unrefined substances in Figure 4. The molecule size decrease to go through a #200 ASTM sifter (75 µm) for both GGBFS and Red-Mud was accomplished through crushing utilizing a Retsch processor.

(a) (b)

Figure 4. (a) GGBFS, (b) Red-Mud (Aluminium slag) as Powder

2.3.3. Pozzolanic Activity Index

The hydraulic reactivities of the utilized geopolymer binders (GGBFS and Red-Mud) were evaluated using hydrated lime $Ca(OH)_2$ as an alkaline activator. Each ground dried solid was blended in the dry state with a solid: $Ca(OH)_2$ ratio of 80:20, respectively. The hydration process was initiated by a mixing ratio of 1:1 by weight. The kinetics of hydration were investigated by determining the remaining (unreacted) free lime content as well as the chemically combined water content at various stages of hydration (2 and 6 hours and 1, 2, and 7 days). The residual free lime content during hydration is presented in Table 4.

Table 4. Free lime content remaining during hydration, H means Hours & d means days

Geo-polymer Concrete Binder	CaO, %				
	2 H	6 H	1 d	2 d	7 d
Red Mud	0.43	0.32	0	0	0
GGBFS	7.9	5.8	4.9	3.2	0.39

Based on the obtained results, it is clear that the free lime content decreases as the hydration period increases. This decline is attributed to its utilization through the pozzolanic reaction with each of the examined solids. Clearly, Red-Mud (aluminum slag) demonstrated exceptionally high pozzolanic activity, with all the free lime being consumed within the initial 6 hours of the hydration process. In contrast, GGBFS exhibited moderate pozzolanic activity, as the free lime content was nearly depleted after 7 days of hydration.

2.4. Activator Materials/Solution

The alkaline activators employed included sodium silicate (Na_2SiO_3) and sodium hydroxide (NaOH). The sodium meta-silicate ($Na_2SiO_3.9H_2O$) solution consisted of Na at 16.17%, O at 67.55%, H at 6.38%, and Si at 9.88% by mass. It had a density of 2.4 g/cm^3 and a melting point of 1.088 °C. Sodium meta-silicate, also referred to as high-specific gravity glass water, appears as colorless crystals with a molecular weight (M.W.) of 284.2 g/mol and a purity of 98%. NaOH was in flake shape with a purity of 96%, a density of 2.13 g/cm^3, a temperature at which a substance melts of 318 °C, and a molecular weight (M.W.) of 40 g/mol. Please note that preparing sodium silicate alkaline in liquid form from sodium meta-silicate ($Na_2SiO_3.9H_2O$) (in particle form) requires high temperatures and an extended period. Thus, initially obtaining and utilizing it in liquid form is more convenient. For instance, a 50-kg package of sodium silicate alkaline can be acquired from Morgan Speciality Chemicals Company, located in Al Obour, Egypt.

An alkaline activator composed of Na_2SiO_3 (glass water) and NaOH solution was utilized. The primary factors investigated in this research included the molarity of the NaOH solution and the ratios of [Na_2SiO_3/NaOH]. A single concentration was utilized. The study examined NaOH concentrations at 8 molarity (M). The Na_2SiO_3/NaOH ratio was maintained at 1. Sodium hydroxide solutions were prepared separately and allowed to stand for 24 hours before being mixed with sodium meta-silicate. The mixtures of sodium hydroxide and sodium metasilicate solutions were allowed to stand for one day before being used in the geopolymerization process.

2.5. Additives (SP)

Sikament-163M complied with ASTM C-494 Type A & F standards. [42]. A dosage equivalent to 2.5% of the weight of cementitious material was employed.

2.6. Water

The drinking water sticks to the principles of ASTM C109 [43]. Consumable water was used for both blending the dry materials and relieving the substantial examples. The water-to-solidify proportion (W/C) stayed predictable for all blends at 0.35.

3. Geo-Polymer Fresh Mortar Properties

Firstly, according to workability, the flow table test was used to measure the mortar flow diameter percentage (%) as an indicator of workability, according to ASTM C230 [44], where [flow diameter percentage % = (average diameter of mortar mixtures – 100) / (100)]. OPC mortar with a flow table of 63% shows higher workability than GGBFS or red-mud geopolymer mortars; this may refer to the higher viscosity of the NaOH and Na_2SiO_3 alkaline solutions used in different geopolymer mixtures.

Increasing the NaOH molarity resulted in reducing of the mortar's flowability. Increasing the Na_2SiO_3/NaOH ratios also resulted in a reduction in mortar flowability.

Secondly, according to the mortar bar expansion "Accelerated Mortar Bar Test (AMBT)," all of the used geopolymer materials (GGBFS or Red-Mud) or cement and the sand were first mixed together in a “Technotest” mixer for about 2 minutes. The liquid component of the mixture was then added to the dry materials, and the mixing continued for further about 4 minutes to manufacture and cast fresh mortar bar specimens of 25 × 25 × 285 mm. Mortar bars are submerged in a solution of 1M NaOH that is already at 80 °C for 24 hours in the oven. After that, the initial length of mortar bars is measured as a zero reading with an equipment (a digital dial gauge). Until the next reading, samples remain in 1M NaOH for a period of time, which can be 14 days according to the ASTM C1260-07 standard.

The non-mandatory appendix in ASTM C1260 provides guidance with the following expansion limits: 14-day expansions of less than 0.10% are indicative of “innocuous” behavior, whereas 14-day expansions of more than 0.20% are indicative of “potentially deleterious” expansion. Aggregates with 14-day expansion between 0.10% and 0.20% are known to be either innocuous or deleterious in field performance, and supplemental information in the form of petrographic examination or identification of alkali reaction products in specimens after tests or field service records can be used in the assessment of the performance. OPC with mortar bar expansions of 0.002% and 0.016% shows lower expansion than GGBFS or red-mud geopolymer mortars. This may refer to the finding of the NaOH and Na_2SiO_3 alkaline solutions used in different geopolymer mixtures, which may react chemically with the solution of 1M NaOH (accelerated heat treatment).

4. Geo-Polymer Concrete Mix Design

This research incorporated Ordinary Portland Cement (OPC) concrete as a control mixture for all experiments. The mixture was formulated in accordance with ACI C-211 standards [45]. The desired strength for the OPC concrete control mixes was set at 35 MPa, with a water-to-binder ratio of 0.35. The specific mixture proportions for the control mix are detailed in Table 5.

Table 5. Mix proportions

Mix. Designation	Coarse Agg.	F. Agg.	GGBFS	Red-Mud	OPC	NaOH Solution (kg/m^3)	Na_2SiO_3 Solution
	10 mm	Sand	(kg/m^3)	(kg/m^3)	(kg/m^3)	8 M	(kg/m^3)
Mix. C - Ls	554	647	–	–	408	–	–
Na-Ls-8G	554	647	408	–	–	48	96
Na-Ls-8R	554	647	–	408	–	48	96

4.1. Samples Preparation and Test Methods

Geopolymer concrete was manufactured by blending the dry aggregates with alkaline solutions. Initially, the dry components, including aggregates, GGBFS powder, and Red-Mud, were mixed for 3 minutes until they achieved homogeneity. Subsequently, the solution with the alkaline activator was gradually added to the mixture. Blending was then continued for an additional 4 minutes to expedite the reaction between the dry and liquid components. The resulting mixture exhibits a dark gray hue for the Red-Mud mix and a dark off-white shade for the GGBFS powder mix. Prior to pouring, the fresh mixture underwent a slump test and was then poured into the prepared molds. These molds were internally coated with oil to prevent the mixture from adhering to them. Subsequently, the mixture was compacted for 10 seconds using a compaction rod. Following the casting of the specimens, they were allowed to undergo a resting period at room temperature for one day. The term "Rest Period" denotes the interval from finishing the casting of the test specimen to the onset of curing at an elevated temperature. The compressive strength of geo-polymer concrete cubes rises with age progression. The density of geo-polymer concrete measured approximately 2350 kg/m^3, lower than that of conventional concrete. After 24 hours, the molds were removed, and the specimens were left at room temperature until testing. Similarly, conventional cement concrete specimens were demolded after 24 hours and then subjected to curing. The development of geo-polymer concrete that can cure at ambient temperatures will broaden its potential applications in concrete structures.

4.1.1. Bond Behavior (Pull-Out Test)

Nine-chamber examples of indicated geopolymer substantial blends [three cylinders of (Mix. C - Ls) mixtures, three cylinders of (Na-Ls-8G) mixtures, and others three of (Na-Ls-8R) mixtures] with aspect 30 cm in level and 15 cm breadth with 25 cm implanted length of steel bar. All substantial combination examples were developed and tried under static weakness up to disappointment.

The pullout tests were conducted using the tension hydraulic machine. The applied load was under displacement control conditions. The maximum capacity of the tension machine used was 200 kN. The test was conducted when the specimens were 28 days old. The mean bond stress over the length of rebar embedment can be computed using the applied load (F) on the bar, following the guidelines outlined in ASTM D7913 [46] with the following equation:

$$\tau = \frac{\mathrm{F}}{\pi\, d_b l_e} \tag{1}$$

where τ is Bond stress [MPa], F is Load [N], d_b is Bar diameter [mm], and Embedment length [mm].

4.1.2. Flexural and Shear Behavior

The testing program involves casting and testing six beams, with three subjected to flexural testing and three to shear testing. One beam serves as the control, while two beams are prepared using the optimal geo-polymer GGBFS powder/red-mud mixes for both flexural and shear tests. The beams' dimensions were 100 × 200 × 1400 mm. The flexural beams were configured with an under-reinforced section, featuring reinforcement consisting of 2 bars of #12 at the bottom, 2 bars of #8 at the top, with 8 mm diameter stirrups spaced at 125 mm c/c during the flexural stage. Conversely, during the shear stage, the beams were reinforced with 4 bars of #12 at the bottom, 2 bars of #10 at the top, with 8 mm diameter stirrups spaced at 330 mm c/c. The control concrete beams were labeled as CRC-I and CRC-II. Also, geo-polymer concrete beams are designated as GRC-I/II-Z/RM. Table 6 compiles all the reinforcement and dimension specifications of the beam specimens. Additionally, cubes (100 mm in size). Also, cylinders (100 mm in diameter x 200 mm in height) were cast alongside the beams and subsequently tested. Also, Figures 5-a and 5-b and Figure 6 show a sample of flexural and shear reinforcement beams, respectively. Steel molds for the beam were custom-fabricated for producing the test specimens. The surfaces of the mold, as well as all the cylinder molds, were coated with oil to aid in demolding the specimens. Figure 5 depicts the assembled mold prepared for casting the beam specimens.

Table 6. All reinforcement and dimension details of beam specimens

				Rft. Tensile			
		Beam Des.	**Beam Dim.**	**Comp.**	**Ten.**	**B. Up bars**	**Cover**
Stage I	Flex. Behavior	CRC-I	100 × 200 × 1400 mm	2 # 8	2 # 12	8 # 8 / m	15 mm
		GRC-I-G	100 × 200 × 1400 mm	2 # 8	2 # 12	8 # 8 / m	15 mm
		GRC-I-RM	100 × 200 × 1400 mm	2 # 8	2 # 12	8 # 8 / m	15 mm
Stage II	Shear Behavior	CRC-II	100 × 200 × 1400 mm	2 # 10	4 # 12	3 # 8 / m	15 mm
		GRC-II-G	100 ×200 × 1400 mm	2 # 10	4 # 12	3 # 8 / m	15 mm
		GRC-II-RM	100 × 200 × 1400 mm	2 # 10	4 # 12	3 # 8 / m	15 mm

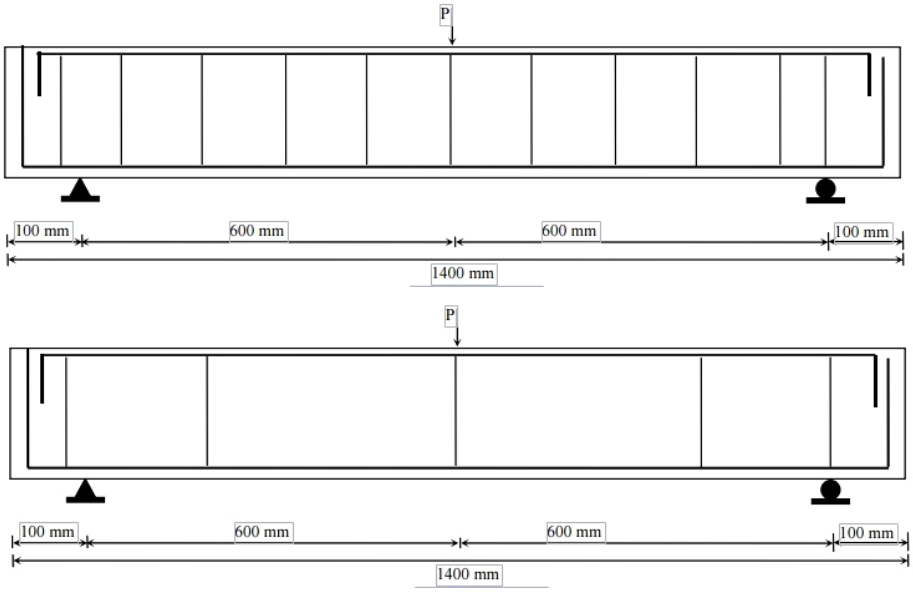

Figure 5. A sample of flexural (a) and shear (b) reinforcement beams

Figure 6. Mold ready to cast the beam specimens

4.1.3. Instrumentation and Test Set-up

The beams underwent testing under a two-point loading configuration with simply supported ends. The specimens were subjected to testing using a loading frame with a capacity of 2000 kN (200 T) and an effective span of 1200 mm. A load unit with a capacity of 200 kN was employed to gauge the applied load. Linear Variable Displacement Transducers (LVDTs) were positioned at the midpoint and beneath the load points of the beam. The load is incremented at intervals of 2.5 kN. LVDT gauges with a count of 0.001 mm are utilized to measure the deflections under the load points and at mid-span. Concrete strain is measured using a strain meter device. A data collection automatically unit is utilized to gather data during the entirety of the test. The initial crack loads were determined through visual inspection. The load is incrementally raised until the specimen fails. The test setup is depicted in Figure 7. The following observations were noted:

- First crack load;
- Displacement at mid span;
- Failure load;
- Crack pattern and failure mode.

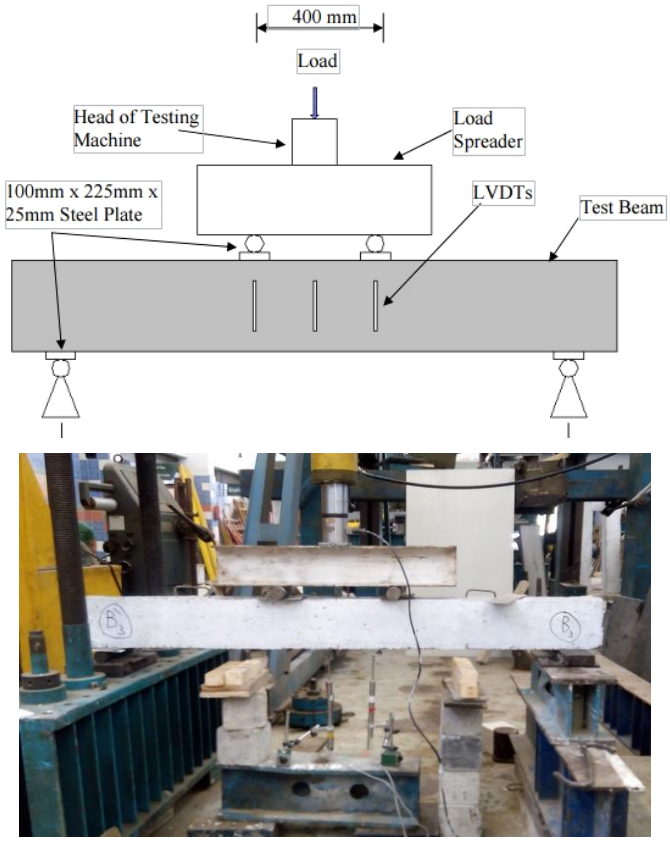

Figure 7. Experimental arrangement for beam testing

5. Results and Discussion

5.1. Bond Behavior

Pull-out tests were conducted using a tension hydraulic machine, and displacement control was employed to apply the load. The maximum capacity of the tension machine used was 200 kN. The test was performed when the specimens reached 28 days of age. The failure load for pull-out and the bond stress measurements of both the control concrete mixture and various samples of optimal geopolymer concrete are detailed in Table 7.

Table 7. All reinforcement and dimension details of beam specimens

Specimens Designation	Average Pull-Out (P)	Embedded Length	Bar Diameter	Bond Strength
	kN	mm	mm	N/mm²
Mix. C - Ls	67.3	250	12	6.80
Na-Ls-8G	53.4	250	12	6.30
Na-Ls-8R	49.4	250	12	6.10

Also, Figure 8 shows the relation between loads and the average result of three pull-out specimens for each case of reinforcement concrete cylinders that have been tested. Also, Figure 9 shows the relation between slippage and the average result of three pull-out specimens for each case of reinforcement concrete cylinders that have been tested.

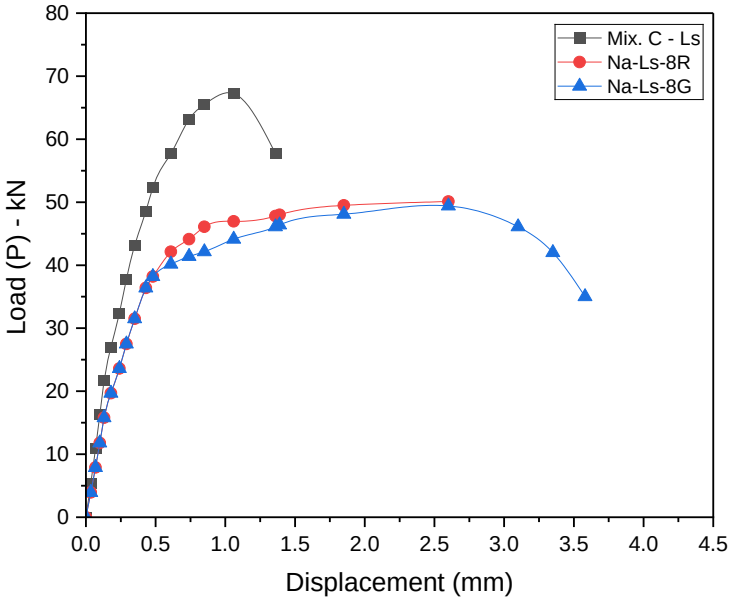

Figure 8. Average (Load-Displacement) for each case of reinforcement concrete cylinders

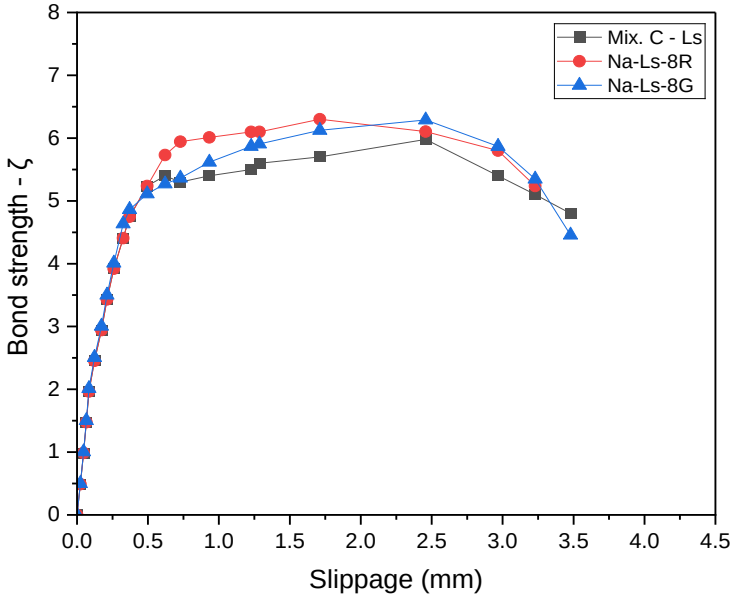

Figure 9. Average (Bond Stress-Slippage) for each case of reinforcement concrete cylinders

Figure 10 shows failure mode of tested specimens and surface crack of pull-out test.

Figure 10. Failure mode of Pull-Out tested specimens

5.2. Flexural Behavior

Three reinforced concrete beams (Mix. C-Ls, Na-Ls-8G, and Na-Ls-8R) were tested under two-point loading. Sufficient shear reinforcement was incorporated within the beam, except in the areas where shear forces were negligible (pure bending regions). Figure 11 depicts the experimental load versus deflection curves for three reinforced flexural beams (Mix. C-Ls, Na-Ls-8G, and Na-Ls-8R). The total span of the beam was 1400 mm, and deflections were recorded at mid-span (X = 700 mm). The deflection responses remained linear with a constant slope until the first flexural crack appeared in all three beams. Following the formation of flexural cracks, variations in the gradient of the load-deflection curves were noted, and the slope of the post-cracking response remained reasonably linear until yielding of the reinforcement occurred. Additionally, Figure 12 illustrates the experimental stress vs. strain curves for three reinforced flexural beams (Mix. C-Ls, Na-Ls-8G, and Na-Ls-8R).

Formation of cracks was marked on the beam during testing. Figure 13 shows the crack pattern and failure modes of (Mix. C-Ls, Na-Ls-8G and Na-Ls-8R) flexural beams, respectively. All beams exhibited of failure by the development of flexural cracks.

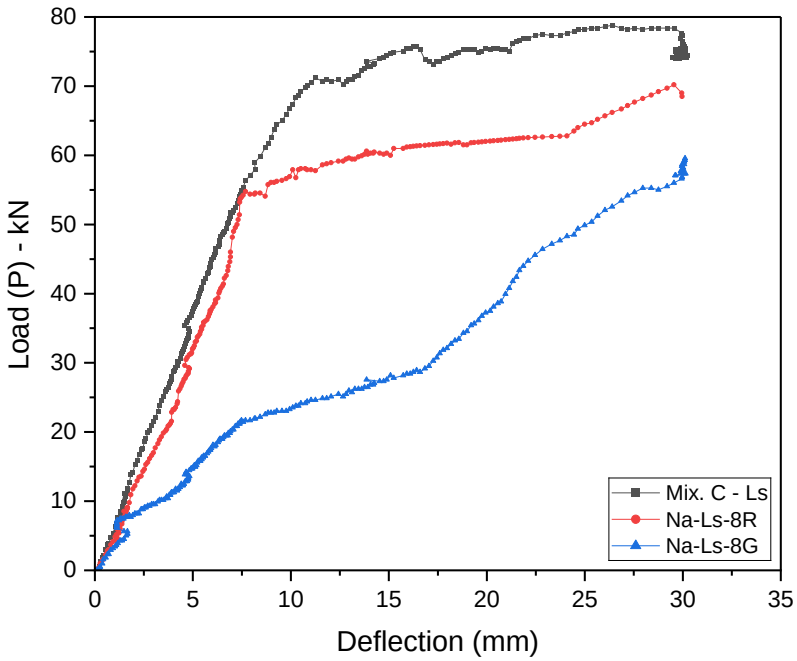

Figure 11. Experimental load vs deflection curves for three flexural reinforced beams

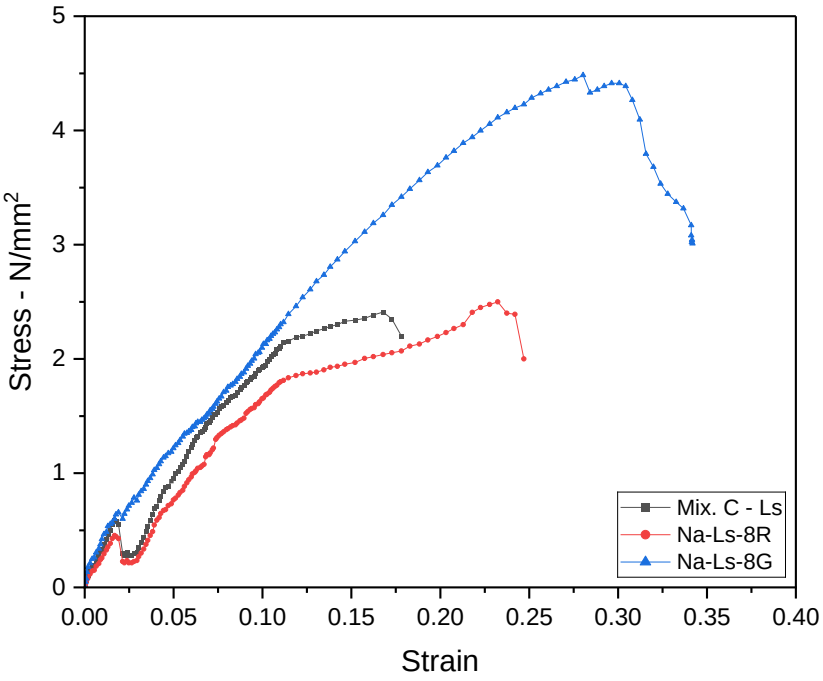

Figure 12. Experimental stress vs strain curves for three flexural reinforced beams

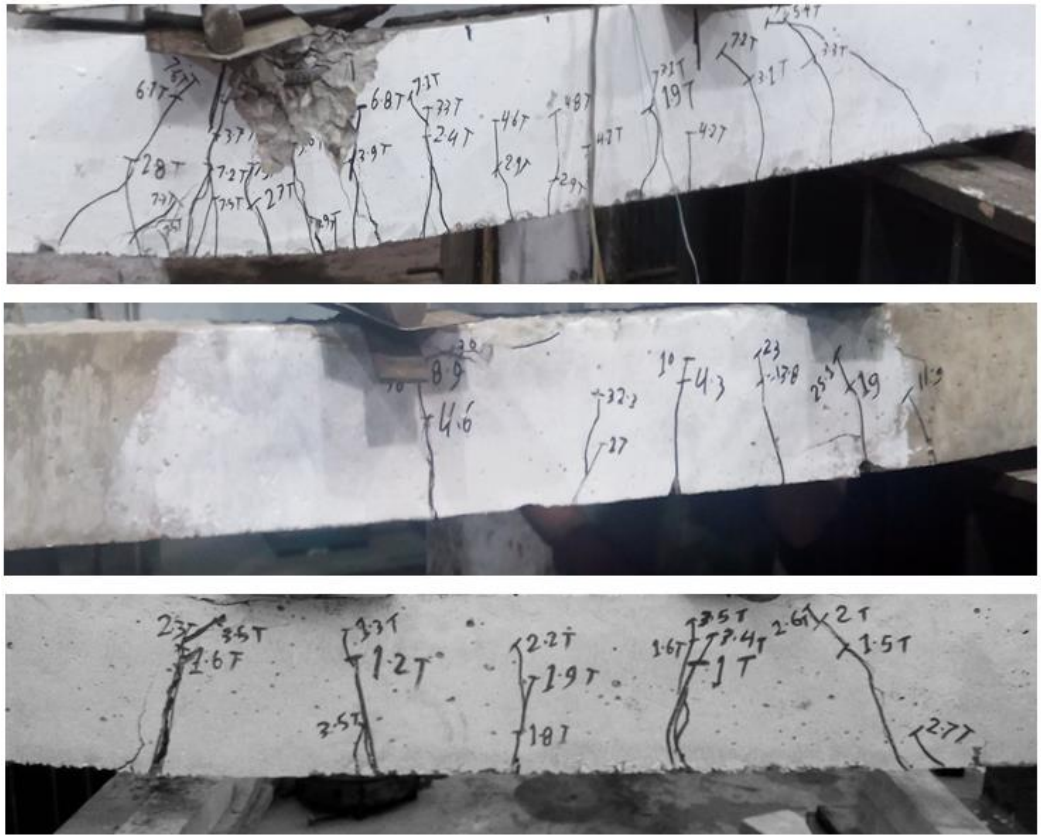

Figure 13. Failure mode for three flexural reinforced beams (Mix. C-Ls, Na-Ls-8G and Na-Ls-8R) respectively

Table 8 summarizes the experimental findings, presenting concrete compressive/flexural strength of (Mix. C-Ls, Na-Ls-8G, and Na-Ls-8R), beam failure modes, and loads at first flexure/diagonal crack, and ultimate load. The initial vertical flexural crack load at mid-span was approximately 7.3 kN, 5.8 kN, and 5.7 kN for the mixed C-Ls, Na-Ls-8G, and Na-Ls-8R beams, respectively, representing about 11% to 12% and 9.5% of their respective ultimate failure loads. Hairline cracks emerged in both the zero shear regions (where the maximum moment occurs) and the shear span as the load increased further. Simultaneously, as the load increased, existing cracks propagated from the bottom of the beam towards the top loading point.

Table 8. Experimental results indicating concrete compressive/flexural strength of different beam mixtures

		Beam Des.	Beam Dim.	Failure Mode	First flexural crack load (KN)	First web shear crack load (KN)	Ult. Load (KN)	% Ult. Load (kN) – According to Control Beam
Stage I	Flex. Behavior	CRC-I	100 × 200 × 1400 mm	Flexural	7.3	Nil	80.2	100
		GRC-I-G	100 × 200 × 1400 mm	Flexural	5.8	Nil	61	74.8
		GRC-I-RM	100 × 200 × 1400 mm	Flexural	5.7	Nil	63	78.6

During the failure stage, cracks extended to the top of the beam within the mid-span region, and failure also ensued within that same region. No shear crack was detected in any of the flexural beams. The failure of the beams, characterized by concrete crushing, occurred long after the flexural reinforcing steels yielded. The failure loads of the beams were 80.2, 63, and 61 kN for the mixed C-Ls, Na-Ls-8G, and Na-Ls-8R beams, respectively.

5.3. Shear Behavior

Experimental tests were conducted to examine the shear behavior of three reinforced beams. Three shear beams without shear reinforcement, namely Mix. C-Ls, Na-Ls-8G, and Na-Ls-8R, were subjected to two-point loading until failure. The ratio of shear span to effective depth (a/d) was maintained at a constant value of 2, and sufficient flexural reinforcement was provided. Figure 14 illustrates the load vs. deflection for the experimented shear beams (Mix. C-Ls, Na-Ls-8G, and Na-Ls-8R) without shear reinforcement. Additionally, Figure 15 depicts the experimental stress vs. strain curves for three reinforced beams (Control Mix 1-Ls, Na-Gr-8Z, and Na-Gr-8R) shear beams.

The change in the slope of the curve signifies a decrease in beam stiffness. Upon reaching the ultimate capacity of shear, a sudden shear failure characterized by brittleness ensued. There was a notable decrease in the load capacity immediately after the shear failure. The ultimate load/shear capacity of the control beam "Mix. C-Ls" was approximately 22% and 11% higher than that of the "Na-Gr-8G" and "Na-Gr-8R" beams, respectively. Additionally, at the maximum load stage, the mid-span deflection for the control beams ranged from 13 to 18 mm, while the "Na-Gr-8G" and "Na-Gr-8R" beams exhibited deflections of 10 mm and 12 mm, respectively. Figure 16 shows the failure mode and cracking pattern in the mixed C-Ls, Na-Ls-8G, and Na-Ls-8R shear beams with shear reinforcement. Furthermore, Figure 16 illustrates the initial crack pattern. Following the development of cracks in the diagonal direction, all beams reinforced with shear RFT displayed a notable load-carrying capacity until failure. The primary diagonal crack typically angles between 25 and 45 degrees, intersecting multiple shear reinforcement bars.

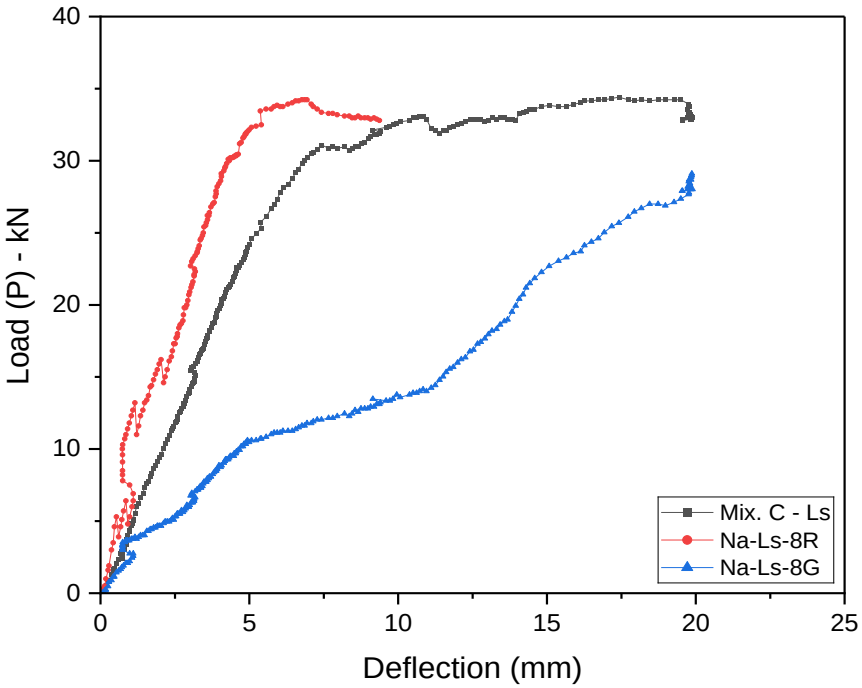

Figure 14. Experimental load vs deflection curves for three shear reinforced beams

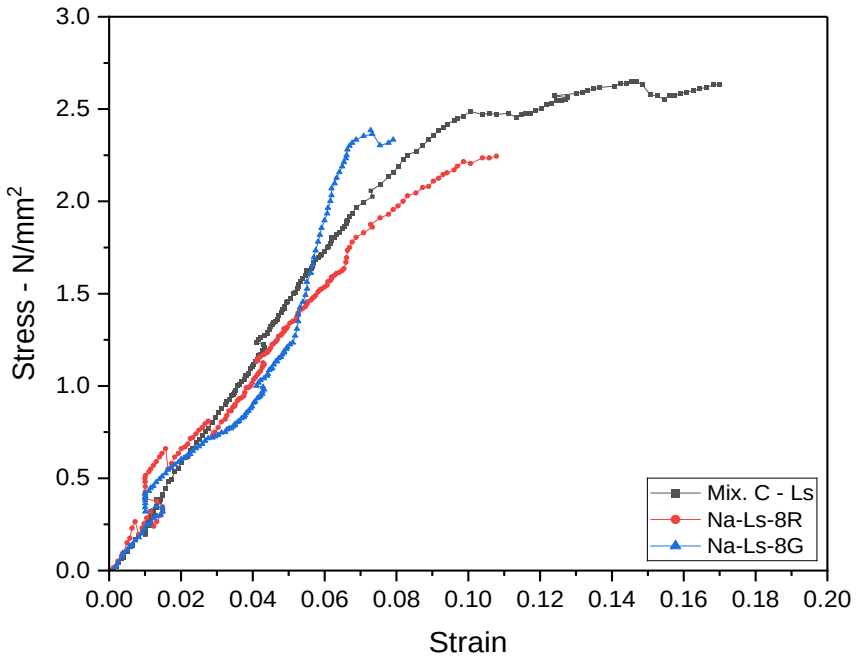

Figure 15. Experimental stress vs strain curves for three shear reinforced beams

Figure 16. Failure mode for three shear reinforced beams (a), (b) and (c), (Mix. C-Ls, Na-Ls-8G and Na-Ls-8R) respectively

Table 9 summarizes experimental results indicating the concrete shear strength of the mixed C-Ls, Na-Ls-8G, and Na-Ls-8R failure modes of the beam and loads at the first diagonal shear crack, the ultimate load. The load at which the which the first diagonal crack occurred was about 17, 16, and 14 kN for the mixed C-Ls, Na-Ls-8G, and Na-Ls-8R beams, respectively, which was about 55% to 65% of their ultimate failure load.

Table 9. Experimental results indicating concrete shear strength of different beam mixtures

		Beam Des.	Beam Dim.	Failure Mode	(a/d) ratio	Flex. Rft. Ratio (ρ)	Shear at first diagonal crack (KN)	Peak/Failure shear (kN)
Stage II	Shear Behavior	CRC-I	100 × 200 × 1400 mm	Shear	2	1.3	19	35
		GRC-I-G	100 × 200 × 1400 mm	Shear	2	1.3	16	27
		GRC-I-RM	100 × 200 × 1400 mm	Shear	2	1.3	14	31

6. In Contrast to Earlier Investigations

Several previous studies and research efforts have investigated the use of geopolymer concrete as a partial or complete replacement for cement. Furthermore, certain studies have examined the viability of utilizing alternative materials such as GGBFS, Class F fly ash, kaolin, or Red-Mud as total substitutes for cement. Table 10 offers a comprehensive compilation that compares the conclusions and presentations from these earlier research endeavors with the results and findings presented in the current study. Maranan et al. [47] stated that, according to the experimental findings, the diameter of the bars did not notably impact the flexural performance of the beams. Typically, increasing the reinforcement ratio enhances the serviceability and performance of a beam. The mechanical interlock and friction forces facilitated by the sand coating were sufficient to ensure a strong bond between the GFRP bars and the geopolymer concrete. Madheswaran et al. [48] stated that the load deflection characteristics at mid-span of the reinforced GPC and OPCC control beams were found to be almost similar. Also, the GPC beams showed slightly more deflection at the same load than the OPCC beams, which is consistent with the results of the current research.

Table 10. A compilation of the most important findings of previous studies used environmentally friendly alternatives to OPC

Authors	Year	Location / Geopolymer type	Geopolymer Materials	Used Activator	Curing Type	Bond Strength	Flexural strength	Shear strength
Current Study	2024	Egypt / Concrete	GGBFS, Red-Mud	NaOH, Na_2SiO_3	Room Temperature	Dec. with av. Value 7%	Dec. with av. Value 4%	Dec. with av. Value 6%
Atis, et al. [19]	2015	Turkey / Mortar	Fly Ash Class F	NaOH	Hot Curing	Nil	Inc. with av. Value 12%	Nil
Raj et al. [34]	2016	India / Concrete	Fly Ash Class F	Na_2SiO_3	Room Temperature	Nil	Dec. with av. Value 3%	Nil
Prasad & Kumar [49]	2017	India / Concrete	GGBFS, Fly Ash Class F	NaOH, Na_2SiO_3	Room Temperature	Not compared with any control mix.		
Aouan et al. [35]	2023	England / Paste and moratar	Kaoline, metakaolin and Fly Ash Class F	NaOH, Na_2SiO_3	Room Temperature	Nil	Nil	Nil
Madheswaran et al. [48]	2015	India / Concrete	GGBFS, Fly Ash Class F	NaOH	Room Temperature	Nil	Dec. with av. Value 9%	Nil

7. Conclusion

The main conclusions, which can be shown from the investigation of chemical properties, physical properties, pozzolanic activity, workability, and expansion of GGBFS and Red-Mud-based geo-polymer mortar, and the investigation of the strength and properties of durability for GGBFS and Red-Mud-based geo-polymer concrete. Also, this presents the main conclusions about the behavior of geo-polymer-reinforced concrete beams under flexural and shear stresses. From the findings and observations made in the preceding tests and their evaluations, it emerged that concrete cured at low or ambient temperatures may exhibit a coarser microstructure characterized by high porosity gel. Elevating the silicate content or alkaline molarity could enhance reactivity, leading to a denser microstructure. Two modes of failure were noted in the tested beams: flexural and shear failure. The observed failure modes and patterns of cracking closely mirrored those reported in previous literature concerning Portland cement concrete beams. The load-deflection curves unmistakably displayed the inception of the initial flexural crack and diagonal crack, aligning with observations reported in prior literature on Portland cement concrete beams. In summary, this investigation illustrated that the computational approaches utilized in determining the shear strength of reinforced Portland cement concrete beams can be effectively applied to forecast the shear strength of reinforced geopolymer concrete beams. The code provisions, typically conservative, remain reliable for estimating the shear strength of geopolymer concrete beams, ensuring safety. Geopolymer cementitious materials are formed through the reaction between alumina-silicate materials and concentrated alkaline solutions, resulting in an inorganic polymer binder. The alkali solutions, characterized by their corrosive nature and often high viscosity, pose challenges in terms of user-friendliness and would present difficulties in large-scale production processes. Future endeavors strive to develop a single-mix geopolymer solution that could serve as a viable alternative to Portland cement when combined with a dry activator, thereby enhancing its commercial viability. The dry activator was mixed with GGBFS and Red-Mud to create geopolymer cement powder, initiating the geopolymerization process upon the addition of water.

8. Declarations

8.1. Author Contributions

Conceptualization, H.M.A., A.A.E., and S.K.; methodology, S.K., A.A.N., and H.M.A.; formal analysis, S.K. and M.S.E.; data curation, A.A.E., H.M.A., and M.S.E.; writing—original draft preparation, S.K.; writing—review and editing, A.A.E. and H.M.A.; supervision, M.S.E. and A.A.N. All authors have read and agreed to the published version of the manuscript.

8.2. Data Availability Statement

The information provided in this study can be obtained upon request from the corresponding author.

8.3. Funding

The authors received no financial support for the research, authorship, and/or publication of this article.

8.4. Acknowledgements

The authors would like to express gratitude to National Research Centre (NRC) for providing the raw materials and carried out all tests.

8.5. Conflicts of Interest

The authors declare no conflict of interest.

9. References

[1] Mehta, A., Siddique, R., Ozbakkaloglu, T., Uddin Ahmed Shaikh, F., & Belarbi, R. (2020). Fly ash and ground granulated blast furnace slag-based alkali-activated concrete: Mechanical, transport and microstructural properties. Construction and Building Materials, 257, 119548. doi:10.1016/j.conbuildmat.2020.119548.

[2] Najimi, M., & Ghafoori, N. (2019). Engineering properties of natural pozzolan/slag-based alkali-activated concrete. Construction and Building Materials, 208, 46–62. doi:10.1016/j.conbuildmat.2019.02.107.

[3] Zhang, H. Y., Yan, J., Kodur, V., & Cao, L. (2019). Mechanical behavior of concrete beams shear strengthened with textile reinforced geopolymer mortar. Engineering Structures, 196(February), 109348. doi:10.1016/j.engstruct.2019.109348.

[4] Rodrigue, A., Duchesne, J., Fournier, B., Champagne, M., & Bissonnette, B. (2020). Alkali-silica reaction in alkali-activated combined slag and fly ash concretes: The tempering effect of fly ash on expansion and cracking. Construction and Building Materials, 251, 118968. doi:10.1016/j.conbuildmat.2020.118968.

[5] Khan, I., Xu, T., Castel, A., Gilbert, R. I., & Babaee, M. (2019). Risk of early age cracking in geopolymer concrete due to restrained shrinkage. Construction and Building Materials, 229, 116840. doi:10.1016/j.conbuildmat.2019.116840.

[6] Kalaivani, M., Shyamala, G., Ramesh, S., Angusenthil, K., & Jagadeesan, R. (2020). Performance evaluation of fly ash/slag based geopolymer concrete beams with addition of lime. Materials Today: Proceedings, 27, 652–656. doi:10.1016/j.matpr.2020.01.596.

[7] Mo, K. H., Alengaram, U. J., & Jumaat, M. Z. (2016). Structural performance of reinforced geopolymer concrete members: A review. Construction and Building Materials, 120, 251–264. doi:10.1016/j.conbuildmat.2016.05.088.

[8] Pol Segura, I., Ranjbar, N., Juul Damø, A., Skaarup Jensen, L., Canut, M., & Arendt Jensen, P. (2023). A review: Alkali-activated cement and concrete production technologies available in the industry. Heliyon, 9(5), 15718. doi:10.1016/j.heliyon.2023.e15718.

[9] Saibaba, K., & Kondraivendhan, B. (2023). Investigation on enhancing the mechanical properties of Alkali-Activated concrete based on fly ash with wollastonite. Materials Today: Proceedings. doi:10.1016/j.matpr.2023.08.120.

[10] Nabavi, F. (2018). Mechanical properties and durability performance of polymer-modified concrete. Fib Symposium, 40, 3493–3503.

[11] Garg, A., Singhal, D., & Parveen. (2019). Review on the durability properties of sustainable alkali activated concrete. Materials Today: Proceedings, 33(3), 1643–1649. doi:10.1016/j.matpr.2020.06.370.

[12] Davidotis, J. (1994). Properties of Geopolymer Cements. First International Conference on Alkaline Cements and Concretes, 11-14 October,1994, Kiev, Ukraine.

[13] Mathew, G., & Joseph, B. (2018). Flexural behaviour of geopolymer concrete beams exposed to elevated temperatures. Journal of Building Engineering, 15, 311–317. doi:10.1016/j.jobe.2017.09.009.

[14] Un, C. H., Sanjayan, J. G., San Nicolas, R., & Van Deventer, J. S. J. (2015). Predictions of long-term deflection of geopolymer concrete beams. Construction and Building Materials, 94, 10-19. doi:10.1016/j.conbuildmat.2015.06.030.

[15] Li, Z., Thomas, R. J., & Peethamparan, S. (2019). Alkali-silica reactivity of alkali-activated concrete subjected to ASTM C 1293 and 1567 alkali-silica reactivity tests. Cement and Concrete Research, 123, 105796. doi:10.1016/j.cemconres.2019.105796.

[16] Saranya, P., Nagarajan, P., & Shashikala, A. P. (2020). Behaviour of GGBS-dolomite geopolymer concrete short column under axial loading. Journal of Building Engineering, 30(December), 101232. doi:10.1016/j.jobe.2020.101232.

[17] Refaie, F. A. Z., Abbas, R., & Fouad, F. H. (2020). Sustainable construction system with Egyptian metakaolin based geopolymer concrete sandwich panels. Case Studies in Construction Materials, 13. doi:10.1016/j.cscm.2020.e00436.

[18] Ahmed, H. Q., Jaf, D. K., & Yaseen, S. A. (2020). Flexural strength and failure of geopolymer concrete beams reinforced with carbon fibre-reinforced polymer bars. Construction and Building Materials, 231, 117185. doi:10.1016/j.conbuildmat.2019.117185.

[19] Atiş, C. D., Görür, E. B., Karahan, O., Bilim, C., Ilkentapar, S., & Luga, E. (2015). Very high strength (120 MPa) class F fly ash geopolymer mortar activated at different NaOH amount, heat curing temperature and heat curing duration. Construction and Building Materials, 96, 673–678. doi:10.1016/j.conbuildmat.2015.08.089.

[20] Hossiney, N., Sepuri, H. K., Mohan, M. K., H R, A., Govindaraju, S., & Chyne, J. (2020). Alkali-activated concrete paver blocks made with recycled asphalt pavement (RAP) aggregates. Case Studies in Construction Materials, 12, 322. doi:10.1016/j.cscm.2019.e00322.

[21] Zhang, P., Wang, K., Li, Q., Wang, J., & Ling, Y. (2020). Fabrication and engineering properties of concretes based on geopolymers/alkali-activated binders - A review. Journal of Cleaner Production, 258, 120896. doi:10.1016/j.jclepro.2020.120896.

[22] Provis, J. L. (2018). Alkali-activated materials. Cement and Concrete Research, 114, 40–48. doi:10.1016/j.cemconres.2017.02.009.

[23] Oyebisi, S., & Alomayri, T. (2023). Artificial intelligence-based prediction of strengths of slag-ash-based geopolymer concrete using deep neural networks. Construction and Building Materials, 400, 132606. doi:10.1016/j.conbuildmat.2023.132606.

[24] Chanda, S. S., & Guchhait, S. (2024). A comprehensive review on the factors influencing engineering characteristics of lightweight geopolymer concrete. Journal of Building Engineering, 86, 108887. doi:10.1016/j.jobe.2024.108887.

[25] Azunna, S. U., Aziz, F. N. A. B. A., Abbas Al-Ghazali, N., Rashid, R. S. M., & Bakar, N. A. (2024). Review on the mechanical properties of rubberized geopolymer concrete. Cleaner Materials, 11, 100225. doi:10.1016/j.clema.2024.100225.

[26] Thomas, R. J., & Peethamparan, S. (2015). Alkali-activated concrete: Engineering properties and stress-strain behavior. Construction and Building Materials, 93, 49–56. doi:10.1016/j.conbuildmat.2015.04.039.

[27] Hassan, H., El-Gamal, S. M. A., Shehab, M. S. H., & Mohsen, A. (2023). Development of green ternary-blended-geopolymers for multifunctional engineering applications. Construction and Building Materials, 409, 133869. doi:10.1016/j.conbuildmat.2023.133869.

[28] Subramanian, S., Davis, R., & Thomas, B. S. (2024). Full-scale static behaviour of prestressed geopolymer concrete sleepers reinforced with steel fibres. Construction and Building Materials, 412, 134693. doi:10.1016/j.conbuildmat.2023.134693.

[29] Martínez, A., & Miller, S. A. (2023). A review of drivers for implementing geopolymers in construction: Codes and constructability. Resources, Conservation and Recycling, 199, 107238. doi:10.1016/j.resconrec.2023.107238.

[30] Tran, T. T., Pham, T. M., & Hao, H. (2020). Effect of hybrid fibers on shear behaviour of geopolymer concrete beams reinforced by basalt fiber reinforced polymer (BFRP) bars without stirrups. Composite Structures, 243, 112236. doi:10.1016/j.compstruct.2020.112236.

[31] Pires, E. F. C., Lima, T. V., Marinho, F. J. V., De Vargas, A. S., Mounzer, E. C., Darwish, F. A. I., & Silva, F. J. (2019). Physical nonlinearity of precast reinforced geopolymer concrete beams. Journal of Materials Research and Technology, 8(2), 2083–2091. doi:10.1016/j.jmrt.2019.01.016.

[32] Abdulkareem, M., Havukainen, J., & Horttanainen, M. (2019). How environmentally sustainable are fibre reinforced alkali-activated concretes? Journal of Cleaner Production, 236, 117601. doi:10.1016/j.jclepro.2019.07.076.

[33] Hassan, A., Arif, M., & Shariq, M. (2020). A review of properties and behaviour of reinforced geopolymer concrete structural elements- A clean technology option for sustainable development. Journal of Cleaner Production, 245. doi:10.1016/j.jclepro.2019.118762.

[34] Raj, S. D., Ganesan, N., Abraham, R., & Raju, A. (2016). Behavior of geopolymer and conventional concrete beam column joints under reverse cyclic loading. Advances in Concrete Construction, 4(3), 161–172. doi:10.12989/acc.2016.4.3.161.

[35] Aouan, B., Alehyen, S., Fadil, M., El Alouani, M., Saufi, H., & Taibi, M. (2023). Characteristics, microstructures, and optimization of the geopolymer paste based on three aluminosilicate materials using a mixture design methodology. Construction and Building Materials, 384, 131475. doi:10.1016/j.conbuildmat.2023.131475.

[36] Lekshmi, S., Sudhakumar, J., & Thomas, S. (2023). Application of clay in geopolymer system: A state-of-the-art review. Materials Today: Proceedings. doi:10.1016/j.matpr.2023.04.083.

[37] Islam, A., Alengaram, U. J., Jumaat, M. Z., & Bashar, I. I. (2014). The development of compressive strength of ground granulated blast furnace slag-palm oil fuel ash-fly ash based geopolymer mortar. Materials and Design, 56, 833–841. doi:10.1016/j.matdes.2013.11.080.

[38] Visintin, P., Mohamed Ali, M. S., Albitar, M., & Lucas, W. (2017). Shear behaviour of geopolymer concrete beams without stirrups. Construction and Building Materials, 148, 10–21. doi:10.1016/j.conbuildmat.2017.05.010.

[39] Fan, J., Zhu, H., Shi, J., Li, Z., & Yang, S. (2020). Influence of slag content on the bond strength, chloride penetration resistance, and interface phase evolution of concrete repaired with alkali activated slag/fly ash. Construction and Building Materials, 263, 120639. doi:10.1016/j.conbuildmat.2020.120639.

[40] ASTM C33/C33M-18. (2023). Standard Specification for Concrete Aggregates. ASTM International, Pennsylvania, United States. doi:10.1520/C0033_C0033M-18.

[41] ASTM C618-12a. (2012). Standard Specification for Coal Fly Ash and Raw or Calcined Natural Pozzolan for Use in Concrete. ASTM International, Pennsylvania, United States.

[42] ASTM C494/C494M-17. (2017). Standard Specification for Chemical Admixtures for Concrete. Annual Book of ASTM Standards. ASTM International, Pennsylvania, United States.

[43] ASTM C109/C109M. (2020). Standard Test Method for Compressive Strength of Hydraulic Cement Mortars (Using 2-in. or [50-mm] Cube Specimens). ASTM International, Pennsylvania, United States. doi:10.1520/C0109_C0109M-20.

[44] ASTM C230/C230M-20. (2021). Standard Specification for Flow Table for Use in Tests of Hydraulic Cement. ASTM International, Pennsylvania, United States. doi:10.1520/C0230_C0230M-20.

[45] Prestera, J. R., Boyle, M., Crocker, D. A., Chairman, S. B., Abdun-Nur, E. A., Barton, S. G., ... & Yuan, R. L. (1998). Standard Practice for Selecting Proportions for Structural Lightweight Concrete (ACI 211.2-98). Reported by ACI Committee 211, American Concrete Institute, Michigan, United States.

[46] ASTM D7913/D7913M-14 (2020). Standard Test Method for Bond Strength of Fiber-Reinforced Polymer Matrix Composite Bars to Concrete by Pullout Testing. ASTM International, Pennsylvania, United States. doi:10.1520/D7913_D7913M-14R20.

[47] Maranan, G. B., Manalo, A. C., Benmokrane, B., Karunasena, W., & Mendis, P. (2015). Evaluation of the flexural strength and serviceability of geopolymer concrete beams reinforced with glass-fibre-reinforced polymer (GFRP) bars. Engineering Structures, 101, 529–541. doi:10.1016/j.engstruct.2015.08.003.

[48] Madheswaran, C. K., Ambily, P. S., Dattatreya, J. K., & Ramesh, G. (2015). Experimental studies on behaviour of reinforced geopolymer concrete beams subjected to monotonic static loading. Journal of the institution of engineers (India): Series A, 96, 139-149. doi:10.1007/s40030-015-0115-1.

[49] Prasad, N. D., & Kumar, Y. H. (2017). Study of behaviour of geo-polymer concrete with respect to its mechanical properties of GGBS and flyash. International Journal of Civil Engineering and Technology, 8(2), 264–273.